ICAS 2016
30th Congress of the International Council of the Aeronautical Sciences
DCC, Daejeon, Korea ; September 25-30, 2016

NUMERICAL INVESTIGATION OF FAN-BLADE OUT USING MESO-SCALE COMPOSITE MODELING

Brandon Horton*, Javid Bayandor*
***CRashworthiness for Aerospace Structures and Hybrids (CRASH) Lab, Virginia Tech**

Keywords: *Fan-blade out, Meso-scale modeling, Softwall casing*

Abstract

The effects of ingesting foreign bodies or other fragments into an engine is a major hazard that could potentially result in a blade-out event. Due to the high rotational speeds, an ejected fan blade can pose an even greater risk than the original foreign body, necessitating the current certification requirements. As such a test is prohibitively expensive, effective computational analysis to simulate a fan-blade out scenario is necessary. The current work investigates a fan-blade out scenario that is consistent with certification requirements for a modern high-bypass engine. Emphasis is placed on two casing designs that incorporate a Kevlar 29 overwrap while a fully Ti-6Al-4V casing serves as a baseline. A meso-scale approach is used for the composite modeling, which is validated against a ballistic experiment for three different composite damage theories. In addition to comparing the response of a conventional and composite fan casing, the effect of bonding between Kevlar layers is explored.

1 Introduction

In the event of a foreign body ingestion scenario, fatigue failure, or manufacturing defect, a commercial engine must demonstrate the capability to contain any released blades or fragments. This test, required by FAR 33.94 [1], must occur for the stage with the highest blade-release energy, which is typically the fan blade for high-bypass engines [2]. However, due to the extreme cost required to conduct and instrument such a test, significant research has been directed toward computationally modeling.

Most early works [3–6] used analytical or single-blade models to evaluate containment response for steel cylinders, giving general approximations of expected casing deformation. Building on the previous works, Sarkar and Atluri [7] considered the effect of multi-blade interactions, discovering that the peak forces exerted on the casing were approximately twice as much as predicted by a single-blade study. Since then, models have progressively become more complex. Shmotin et al. [8] used a high-fidelity fan model to investigate computational modeling effects such as instantaneous blade release and mesh density. An alternative casing geometry incorporating a convex curve in the impact region was proposed by Carney et al. [9] and found it to have a higher ballistic limit. Rotational imbalances from blade release have been shown to play a significant role both numerically [10] and experimentally [11], contributing to blade-casing interactions. A recent FAA report [2] highlighted the importance of blade tip friction for predicting blade containment.

In an effort to reduce costs, lightweight composites have been incorporated into turbofan engines. Due to the size and weight of the casing, it has been targeted as a potential way to significantly reduce costs. As a candidate material, Kevlar has been widely studied in an attempt to characterize its behavior for the purpose of ballistic protection. Its anisotropic properties, strain-rate dependency, and inherently multi-scale nature make it a complex material requiring much experimental observation. Researchers such as van Hoof, Cunniff, and Roylance conducted many experimental tests to characterize the impact response of Kevlar. Cunniff identified the longitudinal strain waves that are produced upon projectile impact, propagating from the impact zone at the speed of sound through the material

[12]. This corroborates earlier observations by Freeston and Claus [13] that concluded that the decay of strain waves due to fiber crossover is very small (reflection coefficient of approximately 0.01). Roylance also showed that this small reflectance causes the majority of the stress to be carried by the principal yarns instead of the orthogonal yarns [14]. This ability to involve more material in the impact incident is what gives Kevlar such high energy absorption capability, proving it to be a good protective fabric [15, 16]. Additionally, Kevlar exhibits limited strain-rate dependency [17], making it somewhat simpler to model than other composite fabrics. More recently, Kevlar was extensively studied specifically for fan casing design in [18, 19].

2 Material Model Theory

Computational analysis requires the use of material models to describe the structural response under a load. Models can vary widely in complexity and computational effort; the following section details the implementations used for this study.

2.1 Ti-6Al-4V

Ti-6Al-4V is a commonly used material in aerospace structures for both fan blades and containment. As such, significant research has gone into accurately defining its material properties and corresponding numerical representation [20–23]. The Johnson-Cook model is frequently employed to model the response of Ti-6Al-4V at high-strain rate applications, but requires an equation of state and is computationally expensive.

Therefore, the model was simplified to the computationally inexpensive linear elastic-plastic model. Using the Johnson-Cook constants provided in [20], the effective stress vs. plastic strain response was simulated. From the relatively strain-rate independent response, a linear-plasticity model was approximated as shown in Fig. 1.

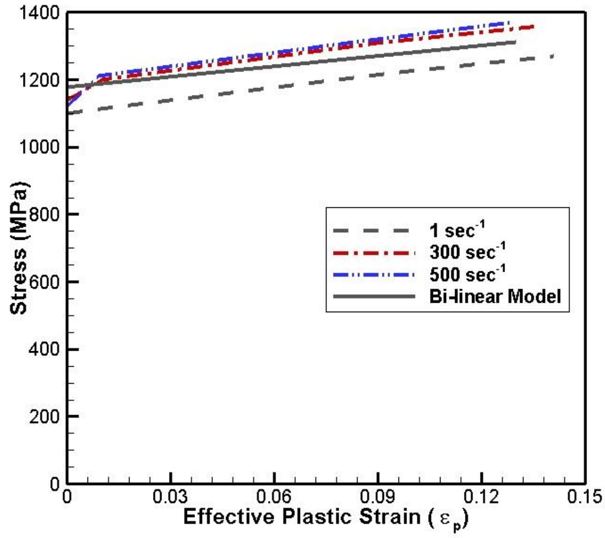

Fig. 1. Stress vs. effective plastic strain response using Johnson-Cook and bi-linear models

2.2 Kevlar 29

The composite overwrap used in this study is composed of Kevlar 29 due to its common use in ballistic applications and available material properties. The parameters used for this study are given in Table 1.

Table 1. Kevlar material properties

Property	**Literature Values** [24, 25]	**Units**
ρ	1230	kg/m^3
E_1	18.5	GPa
E_2	18.5	GPa
E_3	6.0	GPa
ν_{12}	0.25	-
ν_{23}	0.33	-
ν_{13}	0.33	-
G_{12}	0.77	GPa
G_{23}	2.71	GPa
G_{13}	2.71	GPa
ε_f	0.05*	-

*Approximated assuming brittle failure

Many composite damage models exist, so a preliminary numerical validation was performed using three damage models: Chang-Chang, Tsai-Wu, and 3-D orthotropic. The first two are phenomenological models that implement the plane stress assumption and therefore do not account for out-of-plane failure. Their respective formulations can be found in references [26] and [27].

Unlike the previously mentioned models, the 3-D anisotropic model is not based on phenomenological observations. This model considers failure in a three-dimensional stress space where the ultimate failure and damage are purely driven by strain. The damaged compliance matrix is given by Equation 1 where E_{ij} is Young's modulus, v_{ij} is Poisson's ratio, G_{ij} is shear modulus, and d_{ij} is the damage parameter. This damage parameter is active in both tension and compression and updates based on the component strains, as shown in Equation 2:

$$d_{ij} = \max\left(d_{ij}; d_{ij}^{c} \left\langle \frac{\varepsilon_{ij} - \varepsilon_{ij}^{th}}{\varepsilon_{ij}^{c} - \varepsilon_{ij}^{th}} \right\rangle\right) \qquad (2)$$

where ϵ_{ij} is strain, and subscripts c and th represent critical and threshold values respectively. The formulation of the damage parameter ensures that any damage inflicted remains present throughout the simulation.

2.3 Epoxy (Tiebreak)

A meso-scale modeling approach is used for this analysis, allowing delamination to be explicitly modeled. The separation model used for this analysis is the Dycoss Discrete Crack model [28]. This model works in both tension and compression, with shear (σ_s) and normal (σ_n) failure criteria that govern interface strength as show in Equation 3:

$$\left[\frac{\max(\sigma_n, 0)}{\sigma_N}\right]^2 + \left[\frac{\sigma_s}{\sigma_S - \sin(\theta)\min(0, \sigma_n)}\right]^2 = 1 \qquad (3)$$

By allowing separation to be calculated on a continuous scale from 0 to 1, where 0 represents full adhesion and 1 represents full separation, the epoxy stretching between interfaces is simulated.

2.4 Composite model validation

Each of the discussed composite damage models were validated against an experimental ballistic impact test [25] using a meso-scale computational approach. For this preliminary validation, nineteen plies of woven Kevlar 29 were subjected to a 146 m/s impact by a hemispherical nose-shaped projectile.

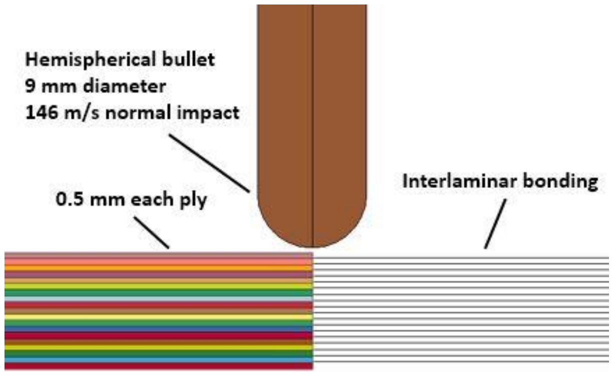

Fig. 2. Setup for composite meso-scale modeling validation

The model cutaway shown in Fig. 2 was simulated for 30.48 x 30.48 mm using a quarter-symmetric assumption. For each damage model, the deformation-time history and delamination progression are recorded and compared against existing literature. All models used the material properties given in Table 1 as inputs.

$$S_{ij}^{dam} = \begin{bmatrix} \frac{1}{E_1(1-d_{11})} & -\frac{v_{21}}{E_2} & -\frac{v_{31}}{E_3} & 0 & 0 & 0 \\ -\frac{v_{12}}{E_1} & \frac{1}{E_2(1-d_{22})} & -\frac{v_{32}}{E_3} & 0 & 0 & 0 \\ -\frac{v_{13}}{E_1} & -\frac{v_{23}}{E_2} & \frac{1}{E_3(1-d_{33})} & 0 & 0 & 0 \\ 0 & 0 & 0 & \frac{1}{G_{23}(1-d_{12})} & 0 & 0 \\ 0 & 0 & 0 & 0 & \frac{1}{G_{31}(1-d_{23})} & 0 \\ 0 & 0 & 0 & 0 & 0 & \frac{1}{G_{12}(1-d_{31})} \end{bmatrix} \qquad (1)$$

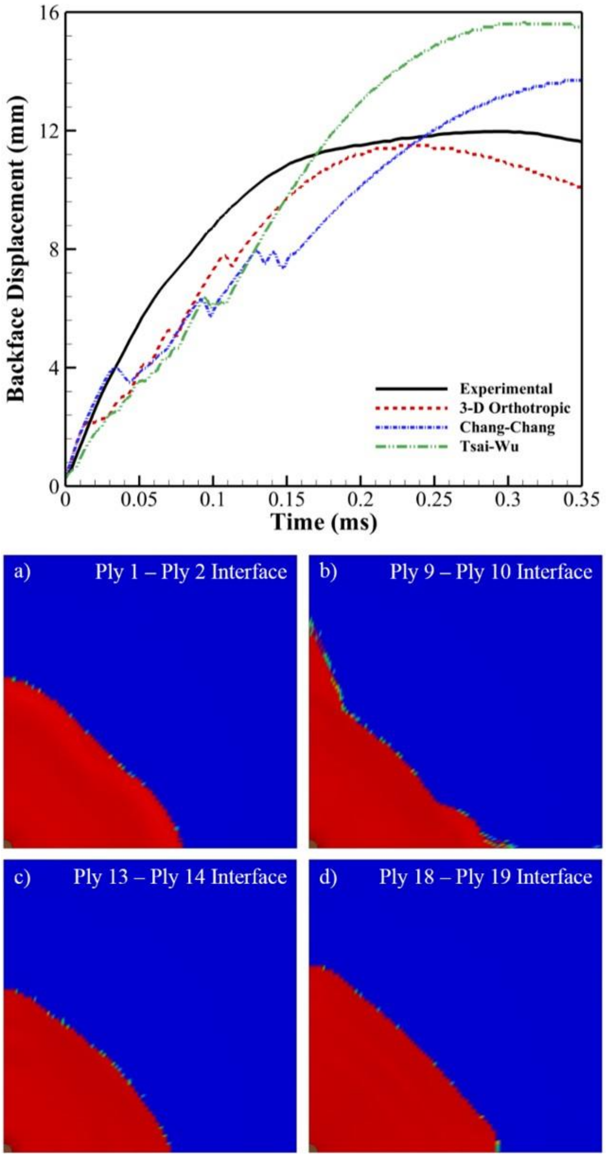

Fig. 3. Backface displacement (top) and delamination area for various plies (bottom)

Figure 3 shows the backface deformation for the selected damage models. Although the slope of displacement was under-predicted by all of the investigated models, both the Chang-Chang and 3-D orthotropic damage models were able to capture the deformation history with acceptable accuracy. The bottom of Fig. 3 displays the delamination area at peak backface deformation for selected plies within the laminate. The delamination shape shown closely matches experiments by [29] and analytical predictions by [30], further validating the capability of the meso-scale modeling approach.

3 Model Development

After validating the meso-scale approach, the full-scale model shown in Fig. 4 was created to simulate a fan-blade out scenario. A generic modern high-bypass turbine engine was used for the analysis, incorporating an axle, full casing, and eighteen wide-chord fan blades. The blades are based on the modern Ti-6Al-4V hollow fan blades, with each having a mass of 12 kg [31]. The casing is also constructed using Ti-6Al-4V and the overwraps are woven Kevlar 29 with the same properties from Table 1. Three casing reinforcement rings are implemented, with one on each side of the fan track and another at the leading edge of the casing. The scenario simulates take-off conditions at max thrust, with the blade out occurring at 2166 RPM and flight speed of 330 km/h. A similar model is more thoroughly discussed in [32].

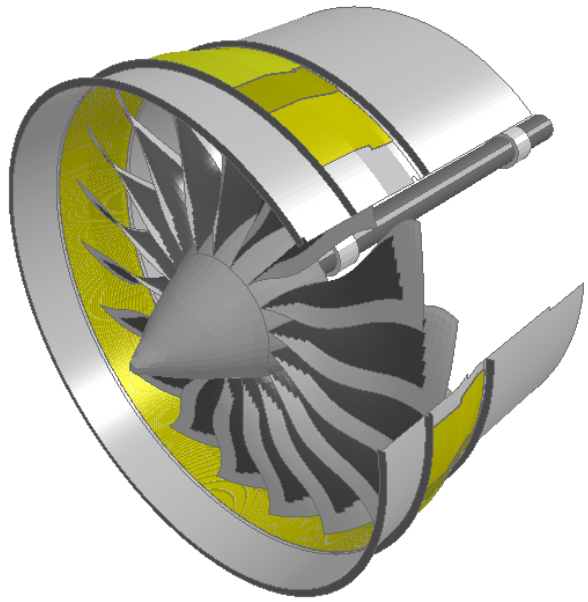

Fig. 4. Cutaway of fan-blade out model with Kevlar 29 overwraps

To improve model fidelity without increasing computational cost, several boundary conditions were introduced. A small section at the top of the casing was fixed to approximate the engine mount on wing, preventing rotation of the casing. A thin ring at the rear of the casing was also fixed to represent the support provided by the exhaust vanes. Shell elements were used to model the blades, axle, and metal sections of the casing, while solid elements were used for all composite layers. Due to the length scales required for such an analysis, each Kevlar overwrap represents ten plies (0.5 mm each ply), with a bonding interface between each overwrap. Without aerodynamic loads, the ejected blade continues to scrape around the inside of the casing, artificially producing more damage. Therefore, upon detachment, an acceleration based on the expected thrust output is applied to the free fan-blade. Finally, the rotational speed of fan assembly is allowed to freely dissipate as the scenario progresses, simulating an automatic engine shutdown due to the rotational imbalance.

4 Fan-blade out investigation

Three casing designs were considered for the fan-blade out analysis: fully titanium casing, titanium with an un-bonded Kevlar overwrap, and titanium with a bonded Kevlar overwrap. The fully titanium casing is used as a baseline case to compare against for weight and damage containment. Each of these scenarios represents potential options for casing design and does not necessary represent a fully optimized design. The sequential damage progression for each design is shown in Fig. 5, with descriptions provided in the following sections.

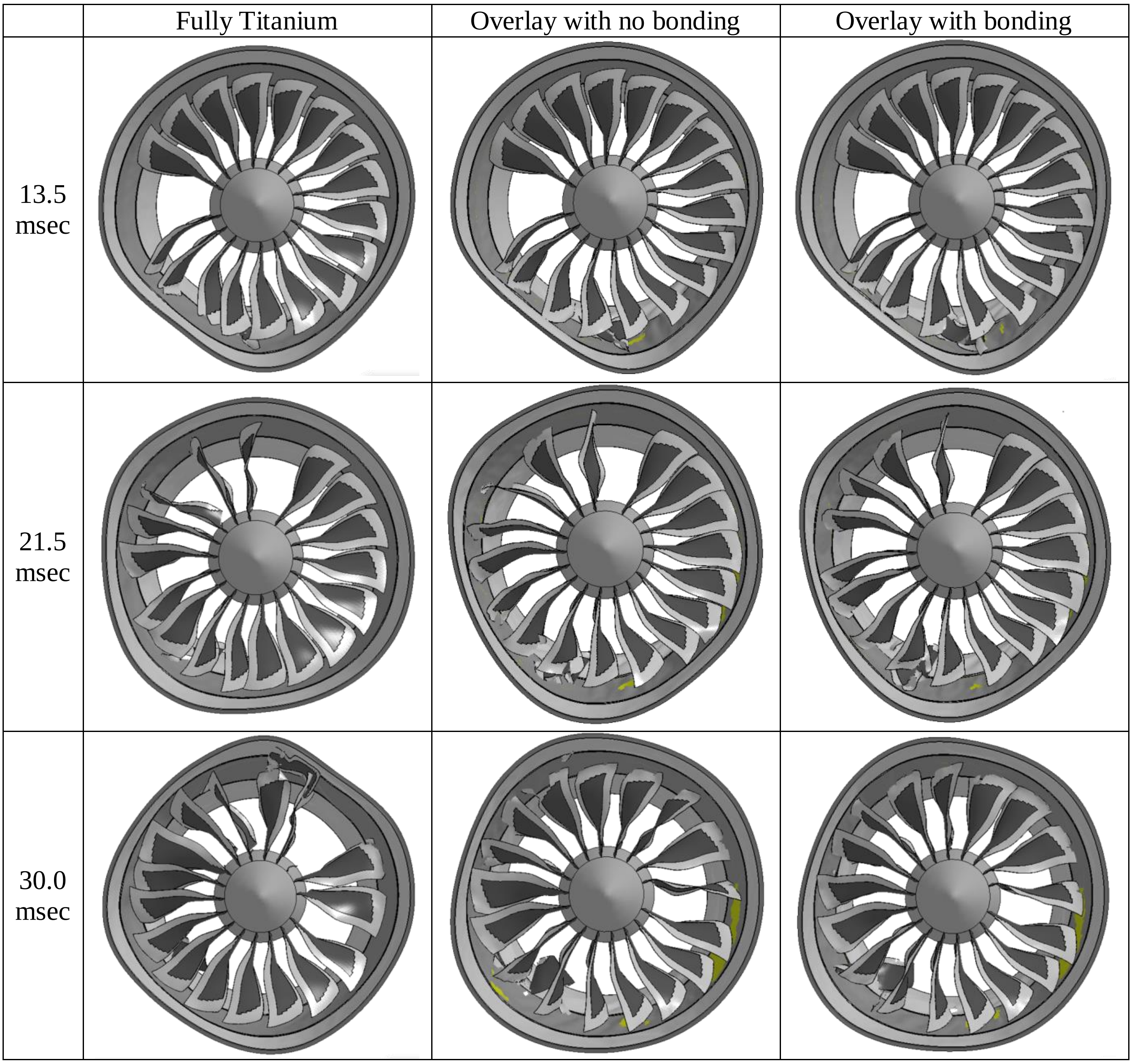

Fig. 5. Sequential damage response for each casing design scenario

4.1 Fully titanium casing

The standard, fully titanium casing was designed with a uniform thickness of 5 mm, resulting in a total casing mass of 398 kg. Upon impact, the fan blade immediately folds while sliding against the inside of the casing. The adjacent blade contacts the detached blade at approximately 50% of the blade height, causing it to crack and eventually break into multiple fragments. By wedging between the fan assembly and casing, the detached blade causes the blade tip and trailing edge of the eight following blades to slightly deteriorate before the detached blade is pushed out of the fan track. Additionally, the deformation applied to the casing causes further blade-casing interaction, contributing to blade tip erosion and applying large bending loads to the blade roots. Due to the loading, the third blade behind the original detachment actually fails at the root, resulting in a secondary blade-out. Despite the damage to the blade tips and secondary blade-out, no penetration of the casing occurs.

4.2 Kevlar overwrap (no bonding)

For the second scenario, the titanium casing was sectioned into different thicknesses, with the thickness along the fan track only 1 mm and 2.5 mm everywhere else. Thirty layers of Kevlar 29 were used as an overwrap around the fan track. Due to the reduced titanium and lightweight composite, the total casing mass was only 273 kg, 31.4% lower than the conventional casing design. Both Chang-Chang and 3-D orthotropic damage models were used to model the Kevlar overwraps, but produce nearly the same response, so only the 3-D orthotropic response is shown.

The wrapped casing is less stiff than the conventional casing, deforming more upon impact. Soon after impact, the titanium lining around the detached blade is compromised, exposing the Kevlar overwrap. This liner restricts the movement of the detached blade, causing contact with the ten following blades. Despite staying longer in the fan track, which causes more fan tip deterioration, the greater deformation of the wrapped casing reduces the contact area on the following fan blades. Additionally, the compromised liner allows greater clearance between the fan assembly and casing wall, decreasing the casing-blade interaction. The reduction in bending loads applied to the blade roots prevents a second blade-out from occurring. Despite further erosion of the titanium lining from blade-casing interaction caused by the casing deformation, no direct damage is caused to the Kevlar overwrap.

4.3 Kevlar overwrap (with bonding)

For the final scenario, the Kevlar overwraps were bonded together, simulating the use of an epoxy or other cured resin. This bonding slightly increases the overall stiffness of the wrapped casing, and allows energy to be dissipated through delamination in addition to deformation.

The response of the bonded casing is almost identical to that of the un-bonded casing, with minor differences in tip erosion and distribution of liner degradation. With a more optimized design a more significant difference could possibly be discerned, but further analysis is required.

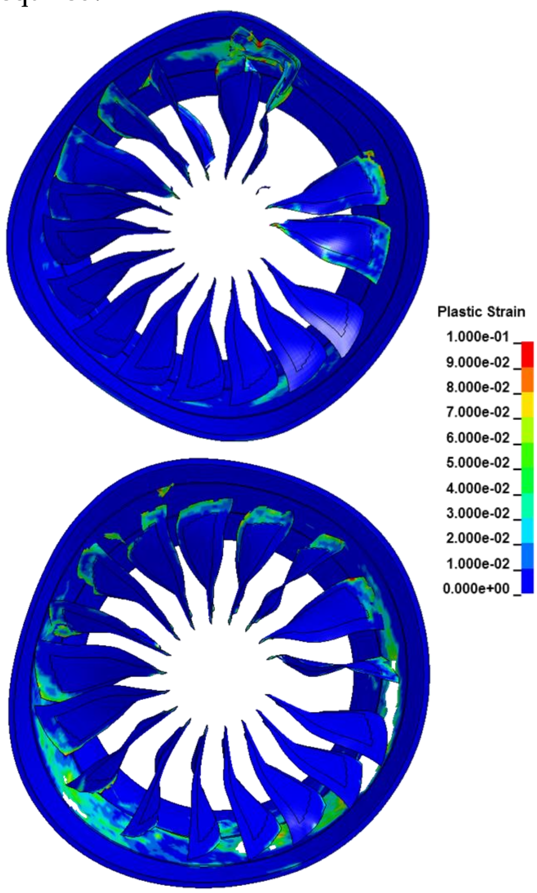

Fig. 6. Plastic strain contour for conventional and wrapped casing designs

4.4 Overall comparison

Both wrapped casing designs provide lightweight alternatives to the conventional fully metal casing. In addition to being lightweight, the wrapped casing designs provide more effective energy dissipation by having a lower overall stiffness and allowing the titanium inner lining to plastically deform and erode. The plastic deformation of the casing and blades for each design are displayed in Fig. 6. Due to the similar response between the two overwrap designs, only the un-bonded case is shown. Until the secondary blade detachment for the conventional casing, the energy dissipation by the casing was 75.4% greater for the overwrap design than for the fully titanium casing. By dissipating more kinetic energy, the loading at the blade roots was reduced, preventing the secondary blade-out from occurring.

5 Conclusions

In this study, a fan blade-out scenario consistent with FAA certification requirements was simulated using a representative high-bypass engine. Three casing designs were used, with one conventional Ti-6Al-4V casing and two softwall, Kevlar 29 casings. The material models used for this study were validated against existing literature before being incorporated into the full-scale blade-out scenario. By using a bi-linear titanium material model, computational time was mitigated while still achieving a close match to an established Johnson-Cook model. The meso-scale composite model was successfully validated against a ballistic experiment for both Chang-Chang and 3-D orthotropic failure theories. The full-scale engine model incorporated eighteen fan blades and a full casing, allowing for multi-blade interaction.

The conventional casing contained the fan blade-out event, but produced a secondary blade-out due to large bending loads imposed at the blade root from the relatively stiff response. Despite having 31.4% less mass, the overwrap casing designs also fully contained the debris. The overall casing stiffness was lower, leading to greater deformation upon impact. However, through the additional casing deformation and erosion of the titanium inner lining, the overwap design dissipated 75.4% more energy, reducing imposed blade root stress and preventing the secondary blade-out. However, no significant difference was observed between the un-bonded and bonded overwrap designs. This could simply mean that the overwrap casing is over-designed, but further research is required.

Future work will more thoroughly investigate each casing design to approach a more optimized result. Due to the non-linear nature of composites, a genetic algorithm could be used to minimize the casing weight while ensuring debris containment. This could also allow the effect of overwrap bonding on the casing to be more clearly defined, potentially improving ballistic response.

References

[1] Advisory Circular, *Engine and Turbosupercharger Rotor Overspeed Requirements of 14 CFR 33.27*. Federal Aviation Administration, 2011.

[2] K. Sengoz, S. Kan, and A. Eskandarian, “Development of a Generic Gas-Turbine Engine Fan Blade-Out Full-Fan Rig Model,” 2015.

[3] A. C. Hagg and G. O. Sankey, “The Containment of Disk Burst Fragments by Cylindrical Shells,” *J. Eng. Power*, vol. 96, no. 2, p. 114, 1974.

[4] R. W-H Wu and E. A. Witmerf, “Approximate Analysis of Containment/Deflection Ring Responses to Engine Rotor Fragment Impact,” *J. Aircr.*, vol. 10, no. 1.

[5] J. H. Gerstle, “Analysis of Rotor Fragment Impact on Ballistic Fabric Engine Burst Containment Shields,” *J. Aircr.*, vol. 12, no. 4.

[6] J. Mathis, S. Parduhn, and P. Alvarez, “Analysis of turbine engine rotor containment and shielding structures,” in *29th Joint Propulsion Conference and Exhibit*, 1993.

[7] S. Sarkar and S. N. Atluri, “Effects of multiple blade interaction on the containment of blade fragments during a rotor failure,” *Finite Elem. Anal. Des.*, vol. 23, no. 2–4, pp. 211–223, Nov. 1996.

[8] Y. N. Shmotin, D. V Gabov, A. A. Ryabov, S. S. Kukanov, and V. N. Rechkin, “Numerical Analysis of Aircraft Engine Fan Blade-Out.”

[9] K. S. Carney, J. M. Pereira, D. M. Revilock, and P. Matheny, “Jet engine fan blade containment using an alternate geometry,” *Int. J. Impact Eng.*, vol. 36, pp. 720–728, 2008.

[10] R. Jain, “Prediction of Transient Loads and

Perforation of Engine Casing During Blade-Off Event of Fan Rotor Assembly.”

[11] B. Yang, “Blade containment evaluation of civil aircraft engines,” *Chinese J. Aeronaut.*, vol. 26, no. 1, pp. 9–16, 2013.

[12] P. M. Cunniff, “An Analysis of the System Effects in Woven Fabrics under Ballistic Impact,” *Text. Res. J.*, vol. 62, no. 9, pp. 495–509, Sep. 1992.

[13] W. D. Freeston and W. D. Claus, “Strain-Wave Reflections During Ballistic Impact of Fabric Panels,” *Text. Res. J.*, vol. 43, no. 6, pp. 348–351, Jun. 1973.

[14] D. Roylance, “Stress wave propagation in fibres: Effect of crossovers,” *Fibre Sci. Technol.*, vol. 13, no. 5, pp. 385–395, Aug. 1980.

[15] D. Roylance and S.-S. Wang, “Penetration Mechanics of Textile Structures.” 1979.

[16] J. E. Field and Q. Sun, “High-speed photographic study of impact on fibers and woven fabrics,” in *Proceedings of SPIE - The International Society for Optical Engineering*, 1991, vol. 1358, pp. 703–712.

[17] Y. Wang and Y. M. Xia, “Experimental and theoretical study on the strain rate and temperature dependence of mechanical behaviour of Kevlar fibre,” *Compos. Part A Appl. Sci. Manuf.*, vol. 30, no. 11, pp. 1251–1257, 1999.

[18] D. Naik, S. Sankaran, B. Mobasher, S. D. Rajan, and J. M. Pereira, “Development of reliable modeling methodologies for fan blade out containment analysis – Part I: Experimental studies,” *Int. J. Impact Eng.*, vol. 36, no. 1, pp. 1–11, 2009.

[19] Z. Stahlecker, B. Mobasher, S. D. Rajan, and J. M. Pereira, “Development of reliable modeling methodologies for engine fan blade out containment analysis. Part II: Finite element analysis,” *Int. J. Impact Eng.*, vol. 36, no. 3, pp. 447–459, 2009.

[20] D. R. Lesuer, “Experimental Investigations of Material Models for Ti-6Al-4V Titanium and 2024-T3 Aluminum,” 2000.

[21] T. Nicholas, “Dynamic Tensile Testing of Structural Materials Using a Split Hopkinson Bar Apparatus.” 1980.

[22] Y. Zhang, J. C. Outeiro, and T. Mabrouki, “On the Selection of Johnson-cook Constitutive Model Parameters for Ti-6Al-4V Using Three Types of Numerical Models of Orthogonal Cutting,” *Procedia CIRP*, vol. 31, pp. 112–117, 2015.

[23] R. S. Yatnalkar, A. Gilat, and B. Harper, “Experimental Investigation of Plastic Deformation of Ti-6Al-4V under Graduate Program in Mechanical Engineering,” 2010.

[24] V. Hoof, “Modelling o f Impact Induced Delamination in,” 1999.

[25] H. L. Gower, D. S. Cronin, and a. Plumtree, “Ballistic impact response of laminated composite panels,” *Int. J. Impact Eng.*, vol. 35, no. 9, pp. 1000–1008, 2008.

[26] S. W. Tsai and E. M. Wu, “A General Theory of Strength for Anisotropic Materials,” *J. Compos. Mater.*, vol. 5, no. 1, pp. 58–80, 1971.

[27] F.-K. Chang and K.-Y. Chang, “A Progressive Damage Model for Laminated Composites Containing Stress Concentrations,” *J. Compos. Mater.*, vol. 21, no. 9, pp. 834–855, Jan. 1987.

[28] P. Lemmen and G. Meijer, “Failure prediction tool theory and user manual,” 2001.

[29] E. Wu and L.-C. Chang, “Woven glass/epoxy laminates subject to projectile impact,” *Int. J. Impact Eng.*, vol. 16, no. 4, pp. 607–619, Aug. 1995.

[30] N. K. Naik, P. Shrirao, and B. C. K. Reddy, “Ballistic impact behaviour of woven fabric composites: Formulation,” *Int. J. Impact Eng.*, vol. 32, no. 9, pp. 1521–1552, 2006.

[31] “Examination of a Failed Fan Blade Rolls-Royce RB211 Trent 892 Turbofan Engine Boeing 777-300, A6-EMM Examination of a Failed Fan Blade Rolls-Royce RB211 Trent 892 Turbofan Engine Boeing 777, A6-EMM.”

[32] Y. Song and J. Bayandor, “Analysis of Progressive Dynamic Damage Caused by Large Hailstone Ingestion into Modern High Bypass Turbofan Engine,” in *AIAA SciTech 2016*, 2016, pp. 1–14.

Contact Author Email Address

bahorton@vt.edu

Copyright Statement